Resonant frequencies of a rectangular cantilever beam immersed in a fluid

Cornelis A. Van Eysden and John E. Sader

Resonant frequencies of a rectangular cantilever beam immersed in a fluid

Cornelis A. Van Eysden and John E. Sader[a)]
Department of Mathematics and Statistics, University of Melbourne, Victoria 3010, Australia

The resonant frequencies of cantilever beams can depend strongly on the fluid in which they are immersed. In this article, we expand on the method of Elmer and Dreier [J. Appl. Phys. **81**, 7709 (1997)] and derive explicit analytical formulas for the flexural and torsional resonant frequencies of a rectangular cantilever beam immersed in an inviscid fluid. These results are directly applicable to cantilever beams of macroscopic size, where the effects of viscosity are negligible, and are valid for arbitrary mode number. In contrast to low mode numbers, in all cases it is found that the fluid has no effect on the resonant frequencies in the limit of infinite mode number. © *2006 American Institute of Physics*. [DOI: 10.1063/1.2401053]

I. INTRODUCTION

Knowledge of the dynamical response of cantilever beams immersed in fluids is fundamental to numerous applications, including environmental sensing,[1] naval architectural design,[2–4] imaging with nanoscale resolution,[5] and design of microelectromechanical systems.[6] Importantly, the specific fluid properties affecting cantilever dynamics depend strongly on the size of the cantilever. For cantilevers of microscopic size, such as those used in the atomic force microscope (AFM), viscosity plays a dominant role and cannot be neglected.[7] As such, a number of theoretical models[8–13] have been developed to account for viscous effects, which show good agreement with experimental measurements for microcantilevers.[9,14] However, as cantilever dimensions are increased to macroscopic size, viscosity exerts a negligible effect and the fluid can be considered to be inviscid in nature,[7] thus greatly simplifying the analysis and interpretation of measurements.

By approximating a rectangular cantilever beam whose length L greatly exceeds its width b by one that is infinitely long, Chu[15] was able to represent the three-dimensional flow around the cantilever by a two-dimensional flow perpendicular to its major axis. This led to the following simple expression for the flexural resonant frequency of a cantilever in fluid ω_{fluid}:

$$\omega_{\text{fluid}} = \omega_{\text{vac}}\left(1 + \frac{\pi\rho b}{4\rho_c h}\right)^{-1/2}, \tag{1}$$

where ω_{vac} is the resonant frequency in vacuum, ρ_c is the density of the beam, and h is its thickness, which is much smaller than the width b. A similar formula was obtained for the torsional modes. For practical cantilevers (of finite length), Eq. (1) is implicitly valid for the lower order harmonics only, due to the nature of the solution. Significantly, Eq. (1) exhibits excellent agreement with experiments on macroscopic cantilevers for the fundamental mode and the next few harmonics.[2]

More recently, Elmer and Dreier[16] extended this well-known formula to encompass flexural modes of arbitrary mode number but did not consider the torsional modes. By accounting for the three-dimensional nature of the flow field, they showed that fluid inertial loading (added apparent mass) on the cantilever decreases as the mode number increases. This in turn established that the fluid has less of an effect at high mode number than at low mode number. However, their formulation necessitates the use of sophisticated numerical techniques to compute the added apparent mass. In this article, we reexamine and extend this methodology to derive exact analytical formulas for both the flexural and torsional modes of vibration that are valid for arbitrary mode number. These analytical formulas provide the necessary extension of Eq. (1), and its torsional counterpart, to arbitrary mode number which will facilitate the calculation of the resonant frequencies of cantilever beams in fluid.

We begin by reviewing the theory of Elmer and Dreier[16] and provide its extension to the torsional modes. This is followed by details of the analytical solution methodology and presentation of results. A discussion of the physical implications of the theoretical findings will also be given.

II. THEORY

The following analysis is rigorously applicable to rectangular cantilever beams whose length L greatly exceeds their width b. We also only consider the limit where the beam thickness h is much smaller than its width b, see Fig. 1. Unlike the Chu solution [Eq. (1)] however, no restriction is placed on the mode number. Furthermore, we assume that the amplitude of vibration is small so that the equations of motion for the fluid may be linearized[17] and that the fluid is incompressible and inviscid in nature.

A. Background theory

1. Flexural modes

For flexural modes of vibration, the governing equation for the elastic deformation of the beam is[18]

---

a)Author to whom correspondence should be addressed; electronic mail: jsader@unimelb.edu.au
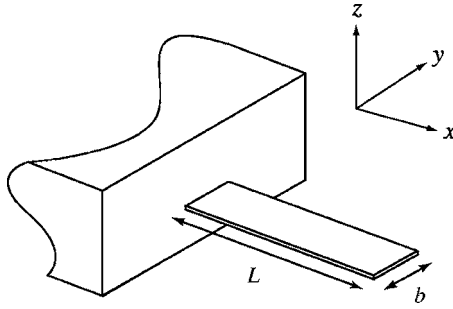
FIG. 1. Schematic illustration showing the plan-view dimensions of a rectangular cantilever. Origin of the coordinate system is at the center of mass of the beam cross section at its clamped end.

$$EI\frac{\partial^4 w(x,t)}{\partial x^4} + \mu\frac{\partial^2 w(x,t)}{\partial t^2} = F(x,t), \tag{2}$$

where $w(x,t)$ is the deflection function of the beam in the z direction, E is Young's modulus, I is the moment of inertia of the beam cross section, μ is the mass per unit length of the beam, $F(x,t)$ is the external applied force per unit length in the z direction, x is the spatial coordinate along the length of the beam, and t is time, see Fig. 1. For a rectangular cantilever beam, $I=bh^3/12$. The corresponding boundary conditions for the cantilever beam are

$$\left[w(x,t) = \frac{\partial w(x,t)}{\partial x} \right]_{x=0} = \left[\frac{\partial^2 w(x,t)}{\partial x^2} = \frac{\partial^3 w(x,t)}{\partial x^3} \right]_{x=L} = 0. \tag{3}$$

To calculate the resonant frequencies of the beam, it is convenient to take the Fourier transform of Eq. (2), for which we obtain

$$EI\frac{d^4\widetilde{w}(x|\omega)}{dx^4} - \mu\omega^2\widetilde{w}(x|\omega) = \widetilde{F}(x|\omega), \tag{4}$$

where

$$\widetilde{X} = \int_{-\infty}^{\infty} Xe^{i\omega t}dt \tag{5}$$

is the Fourier transform of any function X of time and i is the usual imaginary unit. For simplicity we shall henceforth omit this superfluous notation, noting that all dependent variables refer to their Fourier space counterparts. Solving Eq. (4) leads to the well-known result for the vacuum radial resonant frequencies

$$\omega_{\text{vac}}^{(n)} = \frac{C_n^2}{L^2}\sqrt{\frac{EI}{\mu}}, \tag{6}$$

where n is the mode order and C_n is the nth positive root of

$$1 + \cos C_n \cosh C_n = 0. \tag{7}$$

Next, we turn our attention to the load $F(x|\omega)$ applied by the surrounding fluid due to motion of the cantilever. We consider only incompressible inviscid flow, and the governing equations for the fluid in Fourier space are

$$\boldsymbol{u} = -\nabla\phi, \quad \nabla^2\phi = 0, \quad p = -i\rho\omega\phi, \tag{8}$$

where $\boldsymbol{u}$ is the velocity field, ϕ is the velocity potential, p is the pressure, and ρ is the fluid density.

Since the governing beam equation [Eq. (2)] is formally exact in the limit where $L/b \gg 1$, we require a commensurate description of the fluid loading for a mathematically self-consistent formulation. We note that the spatial wavelength of modes along the length of the cantilever is $2\pi L/C_n$, where C_n is defined in Eq. (7). Consequently, the ratio of this wavelength to the cantilever width, i.e., $\alpha_n \equiv (2\pi/C_n)L/b$, dictates the nature of the flow. For small mode numbers n (where $\alpha_n \gg 1$), the flow is two dimensional in nature with the hydrodynamic load per unit length at every point along the cantilever given by that of a rigid beam with identical oscillation amplitude. As such, the load is proportional to the displacement at that point. This property is identical to that used in the formulations of Chu[15] and Sader[7] for the lower order modes. As the mode number n increases, the mode shapes approach a sinusoidal form and the number of nodes along the cantilever also increases. Ultimately, the regime where $\alpha_n \lesssim O(1)$ is reached when the mode number is large, at which point the modes are truly sinusoidal, the flow is three dimensional, and there exists a large number of nodes. For such sinusoidal motion the hydrodynamic load per unit length is again proportional to the displacement, see Sec. II B. As such, the flow is insensitive to end effects in the limit $L/b \gg 1$ regardless of the mode number n, and the hydrodynamic load per unit length is proportional to the local displacement of the beam. From Eq. (8) it then follows that the hydrodynamic load per unit length is given by

$$F(x|\omega) = \frac{\pi}{4}\rho\omega^2 b^2 \Gamma_f(n)w(x|\omega), \tag{9}$$

where ρ is the fluid density and $\Gamma_f(n)$ is the normalized hydrodynamic load (termed the "hydrodynamic function"[7,16]) and depends on the mode order n; in the next section it will be expressed in terms of a normalized mode number since Γ_f also depends on the geometry of the cantilever. The subscript f refers to the flexural mode. We again emphasize that Eq. (9) is formally exact in the limit where $L/b \gg 1$, regardless of the mode number, which is mathematically consistent with the underlying assumptions and use of the beam equation [Eq. (2)]. Substituting Eq. (9) into Eq. (4), it then follows that

$$\omega_{\text{fluid}}^{(n)} = \omega_{\text{vac}}^{(n)}\left[1 + \frac{\pi\rho b}{4\rho_c h}\Gamma_f(n) \right]^{-1/2}. \tag{10}$$

All that remains is to determine the hydrodynamic function Γ_f.

2. Torsional modes

The governing equation for the torsional oscillations of a beam is[18]

$$GK\frac{\partial^2\Phi(x,t)}{\partial x^2} - \rho_c I_p\frac{\partial^2\Phi(x,t)}{\partial t^2} = M(x,t), \tag{11}$$

where $\Phi(x,t)$ is the deflection angle about the major axis of the cantilever, G is the shear modulus, K is a geometric function of the cross section of the beam, I_p is the polar moment of inertia, and $M(x,t)$ is the applied torque per unit length along the beam. For a thin rectangular beam, $K=bh^3/3$ and $I_p=b^3h/12$. The corresponding boundary conditions are

$$\Phi(0,t) = \left.\frac{\partial\Phi(x,t)}{\partial x}\right|_{x=L} = 0. \tag{12}$$

Following a similar analysis to that conducted for the flexural modes, we then find that the resonant frequencies in fluid of a rectangular cantilever beam are

$$\omega_{\text{fluid}}^{(n)} = \omega_{\text{vac}}^{(n)}\left[1 + \frac{3\pi\rho b}{2\rho_c h}\Gamma_t(n)\right]^{-1/2}, \tag{13}$$

where $\Gamma_t(n)$ is the hydrodynamic function for torsional oscillations and is related to the applied moment per unit length by

$$M(x|\omega) = -\frac{\pi}{8}\rho\omega^2 b^4\Gamma_t(n)\Phi(x|\omega), \tag{14}$$

and ω_{vac} is the resonant frequency in vacuum given by

$$\omega_{\text{vac}}^{(n)} = \frac{D_n}{L}\sqrt{\frac{GK}{\rho_c I_p}}, \quad D_n = \frac{\pi}{2}(2n-1), \tag{15}$$

where $n=1,2,3,\ldots$. To complete the formulation, we now examine how the hydrodynamic functions Γ_f and Γ_t can be calculated.

B. Hydrodynamic functions

We note that the displacement functions for the flexural modes of vibration of a cantilever beam are sinusoidal functions of x in the asymptotic limit of high mode order n, and quasisinusoidal for the lowest order modes. All modes are exactly sinusoidal for the torsional modes. From the discussion in Sec. II A, it then follows that the hydrodynamic functions for both flexural and torsional modes can be universally obtained by examining the sinusoidal oscillations of an infinitely long beam. We therefore represent the displacement functions of the infinitely long beam quite generally in terms of the complex exponential function to determine the hydrodynamic functions for arbitrary mode number. The problem then reduces to calculating the flow field driven by such a harmonically oscillating boundary.

As the basis for calculating the flow around a cantilever, we initially consider the flow above an infinite half plane whose surface is executing normal harmonic motion in two orthogonal directions:

$$w(x,y|\omega) = Z_0 e^{ikx}e^{imy}, \tag{16}$$

where the amplitude of oscillation Z_0 is assumed to be much smaller than any other length scale of the flow, leading to linearization of the equations of motion. The motion is therefore purely normal to the surface that lies in the x-y plane, and we remind the reader that all dependent variables corre-

spond to their Fourier transform. The domain containing the fluid ($z>0$) is infinite so we require the velocity field $\boldsymbol{u}$ to vanish as $z\rightarrow\infty$.

It is trivial to derive the velocity potential for this flow problem by solving Eq. (8), from which we find the exact solution

$$\phi(x,y,z|\omega) = -\frac{i\omega Z_0}{\sqrt{k^2+m^2}}e^{ikx}e^{imy}e^{-\sqrt{k^2+m^2}\,z}. \tag{17}$$

The principle of linear superposition can then be used to calculate the flow above a surface executing *arbitrary harmonic motion* with respect to the x and y coordinates. Equation (17) can therefore form the basis for solution of the beam problem. Next, we show how Eq. (17) can be used to reproduce the analysis of Elmer and Dreier,[16] extend it to the torsional modes, and obtain analytical solutions in all cases.

1. Flexural modes

Following from the above discussion, we determine the hydrodynamic function Γ_f by examining an infinitely long beam oscillating with wave number k,

$$w(x|\omega) = Z_0 e^{ikx} \quad \text{where } k = \frac{C_n}{L}, \tag{18}$$

and C_n is given by the solution to Eq. (7). This displacement function ensures that the flow around the beam is antisymmetric about the x-y plane, i.e., the plane of the cantilever $z=0$. Importantly, if $kb\ll 1$, we obtain the result for the oscillation of a rigid beam, whereas for larger values of kb, we recover the result for sinusoidal oscillations, as required in the above formulation for a cantilever beam. This approach therefore enables the hydrodynamic function to be rigorously determined for arbitrary mode number n.

From the no-penetration condition at a solid surface, it follows that the flow field must satisfy the boundary conditions

$$\left.\frac{\partial\phi}{\partial z}\right|_{z=0} = i\omega Z_0 e^{ikx}: |y| \le \frac{b}{2}, \tag{19a}$$

$$\phi(x,y,0|\omega) = 0: |y| > \frac{b}{2}. \tag{19b}$$

Since these conditions are even in the y coordinate, we can use Eq. (17) together with the principle of linear superposition to obtain the following general form for the velocity potential around the cantilever:

$$\phi(\hat{x},\hat{y},\hat{z}|\omega) = i\omega Z_0 e^{i\kappa\hat{x}}\int_0^\infty \chi(\lambda)\cos(\lambda\hat{y})e^{-\sqrt{\kappa^2+\lambda^2}\,\hat{z}}d\lambda, \tag{20}$$

where all coordinates have been scaled by the width of the cantilever such that $\hat{x}=x/b$, $\hat{y}=y/b$, $\hat{z}=z/b$, $\kappa=kb$, and $\lambda=mb$. From Eq. (18), the coefficient κ can be expressed in terms of the aspect ratio of the cantilever such that

$$\kappa = C_n \frac{b}{L}, \tag{21}$$

which shall henceforth be referred to as the "normalized mode number."

The function $\chi(\lambda)$ is to be determined by satisfaction of the boundary conditions in Eq. (19), from which we obtain

$$\int_0^\infty \chi(\lambda)\sqrt{\kappa^2 + \lambda^2}\cos(\lambda\hat{y})d\lambda = 1: |\hat{y}| \le \frac{1}{2}, \tag{22a}$$

$$\int_0^\infty \chi(\lambda)\cos(\lambda\hat{y})d\lambda = 0: |\hat{y}| > \frac{1}{2}, \tag{22b}$$

which are identical to the results obtained by Elmer and Dreier.[16] Importantly, once Eqs. (22) has been solved for $\chi(\lambda)$, Eq. (20) completely specifies the flow field around the beam. This enables the pressure difference between top and bottom surfaces of the beam to be calculated and hence the force per unit length

$$F(x|\omega) = 4\rho\omega^2 b^2 Z_0 e^{i\kappa\hat{x}}\int_0^{1/2}\int_0^\infty \chi(\lambda)\cos(\lambda\hat{y})d\lambda d\hat{y}, \tag{23}$$

which leads to the required result

$$F(x|\omega) = 4\rho\omega^2 b^2 Z_0 e^{i\kappa\hat{x}}\int_0^\infty \chi(\lambda)\frac{\sin(\lambda/2)}{\lambda}d\lambda. \tag{24}$$

From Eqs. (9), (18), and (24) we then obtain

$$\Gamma_f(\kappa) = \frac{16}{\pi}\int_0^\infty \chi(\lambda)\frac{\sin(\lambda/2)}{\lambda}d\lambda. \tag{25}$$

For completeness, results for the pressure distribution over the surface of the beam are given in the Appendix.

We now turn our attention to solving Eqs. (22) for $\chi(\lambda)$. To begin, we follow Ref. 16 and introduce the ansatz

$$\chi(\lambda) = \sum_{m=1}^M a_m \frac{J_{2m-1}(\lambda/2)}{\lambda}, \tag{26}$$

which ensures that Eq. (22b) is identically satisfied. To obtain an analytical solution for the unknown coefficients a_m, however, we take a different approach to Ref. 16 and expand Eq. (22a) as a power series in $\hat{y}$ while noting that the power series expansion of the cosine function has an infinite radius of convergence. Truncating the power series at M terms leads to the following system of equations:

$$\sum_{m=1}^M A_{q,m}a_m = \begin{cases} 1 & : & q = 1 \\ 0 & : & q > 1, \end{cases} \tag{27}$$

where

$$A_{q,m} = \int_0^\infty \lambda^{2q-3}\sqrt{\kappa^2 + \lambda^2}J_{2m-1}(\lambda/2)d\lambda, \tag{28}$$

which can be evaluated exactly to give

$$A_{q,m} = -\frac{4^{2q-2}}{\sqrt{\pi}}G_{13}^{21}\left(\frac{\kappa^2}{16}\middle|\begin{array}{ccc} & & \frac{3}{2} \\ 0 & q+m-1 & q-m \end{array}\right), \tag{29}$$

in terms of the Meijer G-function.[19] Taking the inverse of Eq. (27) yields the unknown coefficients a_m,

$$a_m = A_{m,1}^{-1}, \tag{30}$$

where $A_{m,1}^{-1}$ is the mth row element of the first column in the inverse matrix of $A_{q,m}$. Equations (25) and (26) give the required result

$$\Gamma_f(\kappa) = 2a_1. \tag{31}$$

Finally, we note that $\Gamma_f(\kappa)$ has the following asymptotic solutions:[16]

$$\Gamma_f(\kappa) = \begin{cases} 1 & : & \kappa \to 0 \\ \dfrac{8}{\pi\kappa} & : & \kappa \to \infty, \end{cases} \tag{32}$$

which will be used together with Eq. (31) to formulate an approximate yet simple and highly accurate solution in the next section.

2. Torsional modes

The advantage of the above analysis is that it can be easily extended to the torsional modes of vibration. Whereas the flow field is an even function of $\hat{y}$ for the flexural modes, here it clearly will be an odd function due to the "twisting" motion of the beam about its major axis. To proceed, we consider the angle function of an infinitely long beam oscillating with wave number k,

$$\Phi(x|\omega) = \frac{Z_0}{b}e^{ikx} \quad \text{where } k = \frac{D_n}{L} \tag{33}$$

D_n is given by Eq. (15) and Z_0 is the amplitude of oscillation at the edge of the beam. Again noting that the flow must be antisymmetric about the x-y plane leads to the following boundary conditions:

$$\left.\frac{\partial\phi}{\partial\hat{z}}\right|_{\hat{z}=0} = i\omega Z_0 \hat{y}e^{i\kappa\hat{x}}: |\hat{y}| \le \frac{1}{2}, \tag{34a}$$

$$\phi(\hat{x},\hat{y},0|\omega) = 0: |\hat{y}| > \frac{1}{2}. \tag{34b}$$

Since the flow is an odd function of $\hat{y}$, we obtain the general expression for the velocity potential

$$\phi(\hat{x},\hat{y},\hat{z}|\omega) = i\omega Z_0 e^{i\kappa\hat{x}}\int_0^\infty \zeta(\lambda)\sin(\lambda\hat{y})e^{-\sqrt{\kappa^2+\lambda^2}\hat{z}}d\lambda, \tag{35}$$

where $\zeta(\lambda)$ is to be determined such that Eq. (34) is satisfied; the normalized mode number in this case is

$$\kappa = D_n\frac{b}{L}. \tag{36}$$

Substituting Eq. (35) into Eq. (34) gives

$$\int_0^\infty \zeta(\lambda)\sqrt{\kappa^2+\lambda^2}\sin(\lambda\hat{y})d\lambda = \hat{y}: \ |\hat{y}| \leq \frac{1}{2}, \qquad (37a)$$

$$\int_0^\infty \zeta(\lambda)\sin(\lambda\hat{y})d\lambda = 0: \ |\hat{y}| > \frac{1}{2}. \qquad (37b)$$

Following similar lines to the analysis for the flexural modes, we then find

$$\Gamma_t(\kappa) = \frac{32}{\pi}\int_0^\infty \zeta(\lambda)\left[\frac{\sin(\lambda/2)}{\lambda^2} - \frac{\cos(\lambda/2)}{2\lambda}\right]d\lambda. \qquad (38)$$

To solve Eq. (37) for $\zeta(\lambda)$, we choose an ansatz that automatically satisfies Eq. (37b), namely,

$$\zeta(\lambda) = \sum_{m=1}^M b_m \frac{J_{2m}(\lambda/2)}{\lambda}. \qquad (39)$$

To determine the coefficients b_m, we substitute Eq. (39) into Eq. (37a) and expand $\sin(\lambda\hat{y})$ in its power series. Truncating the power series at M terms leads to the following system:

$$\sum_{m=1}^M B_{q,m}b_m = \begin{cases} 1 & : \quad q = 1 \\ 0 & : \quad q > 1, \end{cases} \qquad (40)$$

where the matrix elements are given by

$$B_{q,m} = -\frac{4^{2q-1}}{\sqrt{\pi}}G_{13}^{21}\left(\frac{\kappa^2}{16}\left|\begin{matrix} & & \frac{3}{2} \\ 0 & q+m & q-m \end{matrix}\right.\right) \qquad (41)$$

in terms of the Meijer G-function.[19] Substituting Eq. (39) into Eq. (38) then gives the required result

$$\Gamma_t(\kappa) = \frac{b_1}{2}. \qquad (42)$$

We now examine the asymptotics of the hydrodynamic function. In the limit $\kappa \to 0$, Eq. (37a) reduces to

$$\int_0^\infty \lambda\zeta(\lambda)\sin(\lambda\hat{y})d\lambda = \hat{y}: \ |\hat{y}| \leq \frac{1}{2}, \qquad (43)$$

whose exact solution is given by the first term in the ansatz, Eq. (39), i.e.,

$$\zeta(\lambda) = \frac{J_2(\lambda/2)}{8\lambda} \quad \text{as } \kappa \to 0. \qquad (44)$$

Substituting Eq. (44) into Eq. (38) then leads to the well-known result of Chu[15]

$$\Gamma_t(\kappa) = \frac{1}{16} \quad \text{as } \kappa \to 0. \qquad (45)$$

In the complementary limit $\kappa \to \infty$, Eq. (37a) becomes

$$\int_0^\infty \zeta(\lambda)\sin(\lambda\hat{y})d\lambda = \frac{\hat{y}}{\kappa}: \ |\hat{y}| \leq \frac{1}{2}, \qquad (46)$$

whose solution can be obtained trivially from the form of Eq. (44). This leads to the required result

$$\Gamma_t(\kappa) = \frac{4}{3\pi\kappa} \quad \text{as } \kappa \to \infty. \qquad (47)$$

The pressure distribution over the surface of the beam is discussed in the Appendix.

In summary, the hydrodynamic functions for the flexural and torsional modes $\Gamma_f(\kappa)$ and $\Gamma_t(\kappa)$ depend only on the entries in the first column and first row of the inverse of the matrices $A_{q,m}$ and $B_{q,m}$ as defined in Eqs. (29) and (41), respectively; the exact solutions are obtained in the limit as $M \to \infty$. Since the entries in these matrices are in terms of analytical functions, the above solutions circumvent the need for using the numerical procedure described in Ref. 16, allowing for direct analytical evaluation and facilitating computation. As will be shown in the next section, these solutions are rapidly convergent with increasing M. To facilitate implementation, a summary of the key analytical results derived above is given in Table I.

III. RESULTS AND DISCUSSION

To begin, we examine the convergence of the analytical solutions for the hydrodynamic functions as the number of terms M is increased. All computations were performed in MATHEMATICA®5.2, where the Meijer G-function is standard. Results of this comparison for the flexural and torsional modes are presented in Fig. 2 using the $M=15$ solutions as references, since these gave identical results to the $M>15$ solutions for the first six significant figures. From Fig. 2 it is clear that the hydrodynamic functions for both flexural and torsional modes converge rapidly to the exact solution as the number of terms increases. The convergence is more rapid for smaller values of κ, since the solutions are exact in the limit of $\kappa \to 0$, for all values of M. Nonetheless, only a few terms are required to achieve convergence of better than 99%.

Having demonstrated convergence of the analytical solutions, we now examine the relative behavior of the flexural and torsional modes for a cantilever immersed in fluid. We note that the hydrodynamic functions for both the flexural and torsional modes depend only on the normalized mode number κ, as defined in Eqs. (21) and (36), respectively. Importantly, both these expressions converge to identical results in the limit of high mode number n and are approximately equal for low mode numbers: $\kappa_{\text{flexural}} = 1.19\kappa_{\text{torsion}}$ for $n=1$ and $\kappa_{\text{flexural}} = 1.00\kappa_{\text{torsion}}$ for $n>1$. As such, the effect of higher order mode numbers on the classical Chu results[15] for the flexural and torsional modes can be examined by directly comparing their hydrodynamic functions for identical values of κ.

A plot of the hydrodynamic functions for the flexural and torsional modes is presented in Fig. 3. Note that both hydrodynamic functions decrease in magnitude as the normalized mode number increases. This indicates that hydrodynamic loading of the surrounding fluid on the cantilever dynamics has less of an effect at higher mode number than at low mode number. As $\kappa \to \infty$, both hydrodynamic functions approach zero, establishing that the resonant frequencies of the cantilever are unaffected by the fluid in the limit of infinite mode number.

TABLE I. Key analytical formulas for calculation of the hydrodynamic functions and resonant frequencies in fluid.

	Flexural modes	Torsional modes
Resonant frequencies	$\omega_{\text{fluid}}^{(n)} = \omega_{\text{vac}}^{(n)}\left[1 + \dfrac{\pi\rho b}{4\rho_c h}\Gamma_f(\kappa)\right]^{-1/2}$	$\omega_{\text{fluid}}^{(n)} = \omega_{\text{vac}}^{(n)}\left[1 + \dfrac{3\pi\rho b}{2\rho_c h}\Gamma_t(\kappa)\right]^{-1/2}$
Normalized mode numbers	$\kappa = C_n\dfrac{b}{L}$	$\kappa = D_n\dfrac{b}{L}$
Eigenvalues	$1 + \cos C_n \cosh C_n = 0$	$D_n = \dfrac{\pi}{2}(2n-1)$
Hydrodynamic functions	$\Gamma_f(\kappa) = 2a_1$	$\Gamma_t(\kappa) = \dfrac{b_1}{2}$
Coefficients a_m, b_m	$\sum_{m=1}^{M} A_{q,m} a_m = \begin{cases} 1 & : & q=1 \\ 0 & : & q>1 \end{cases}$	$\sum_{m=1}^{M} B_{q,m} b_m = \begin{cases} 1 & : & q=1 \\ 0 & : & q>1 \end{cases}$
	$A_{q,m} = -\dfrac{4^{2q-2}}{\sqrt{\pi}}G_{13}^{21}\left(\dfrac{\kappa^2}{16}\Bigg|\begin{matrix}&\frac{3}{2}\\0 & q+m-1 \quad q-m\end{matrix}\right)$	$B_{q,m} = -\dfrac{4^{2q-1}}{\sqrt{\pi}}G_{13}^{21}\left(\dfrac{\kappa^2}{16}\Bigg|\begin{matrix}&\frac{3}{2}\\0 & q+m \quad q-m\end{matrix}\right)$
Pade approximants	$\Gamma_f(\kappa) = \dfrac{1 + 0.742\,73\kappa + 0.148\,62\kappa^2}{1 + 0.742\,73\kappa + 0.350\,04\kappa^2 + 0.058\,364\kappa^3}$	$\Gamma_t(\kappa) = \dfrac{1}{16}\left(\dfrac{1 + 0.379\,22\kappa + 0.072\,912\kappa^2}{1 + 0.379\,22\kappa + 0.088\,056\kappa^2 + 0.010\,737\kappa^3}\right)$

Figure 3 also clearly demonstrates that as the mode number increases, the flexural hydrodynamic function is more strongly affected than the torsional result. Nevertheless, we note that in the limit of infinite mode number $\kappa \to \infty$, the relationship between the resonant frequencies in fluid $\omega_{\text{fluid}}^{(n)}$ and vacuum $\omega_{\text{vac}}^{(n)}$ for the flexural and torsional frequencies are identical, and given by

$$\omega_{\text{fluid}}^{(n)} = \omega_{\text{vac}}^{(n)}\left(1 + \frac{2\rho b}{\rho_c h}\left[\frac{1}{\kappa}\right]\right)^{-1/2}, \quad \kappa \to \infty, \qquad (48)$$

as is evident from Eqs. (10), (13), (32), and (47). This contrasts to the limit as $\kappa \to 0$, where the flexural modes are significantly more affected by immersion in fluid than the torsional modes. This finding demonstrates that the hydrodynamic function for flexural modes is more strongly dependent on mode number than that for torsional modes.

It is important to emphasize that the normalized mode number κ, not the actual mode number n, controls the nature of the hydrodynamic function and hence the effect of fluid on the resonant frequencies. To illustrate this point, consider a cantilever with an aspect ratio $L/b = 10$ whose fundamental flexural mode ($n=1$) has a normalized mode number of $\kappa = 0.2$, whereas $\kappa = 2$ for the $n=10$ higher order flexural mode. Despite the large value of n for the higher order mode, the hydrodynamic function Γ_f for this mode is only 29% lower than that for the fundamental mode. For the torsional modes,
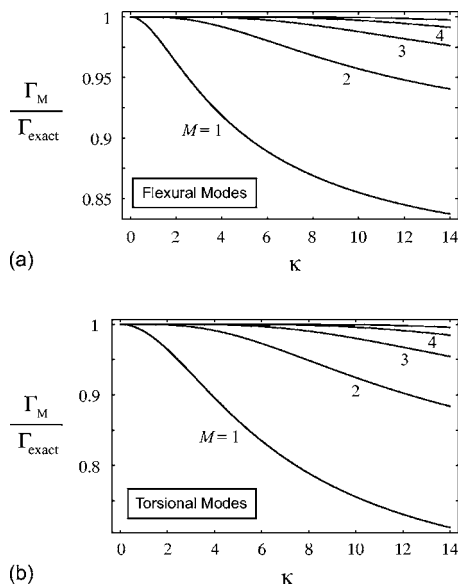

FIG. 2. Convergence of analytical solutions for hydrodynamic functions with increasing number of terms M denoted Γ_M. Reference solution taken as $M=15$ and denoted Γ_{exact}. (a) Flexural modes [Eq. (31)] and (b) torsional modes [Eq. (42)]. Results for $M=1,2,3,4,5$.
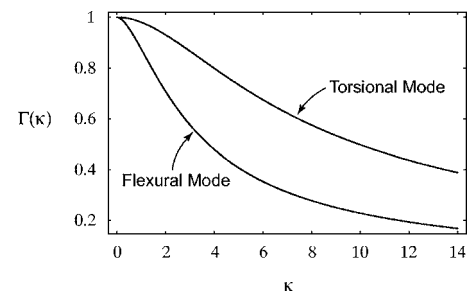

FIG. 3. Hydrodynamic functions $\Gamma_f(\kappa)$ and $16\Gamma_t(\kappa)$ for flexural and torsional modes, respectively, denoted $\Gamma(\kappa)$.
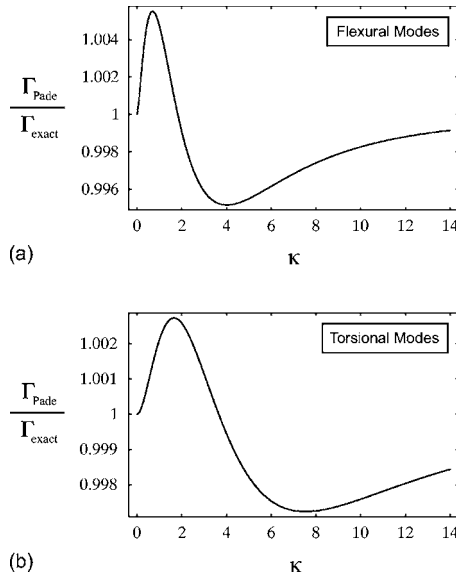
FIG. 4. Accuracy of Padé approximant representations of hydrodynamic functions denoted Γ_{Pade}. Reference solution taken as $M=15$ and denoted Γ_{exact}. (a) Flexural modes [Eq. (50a)] and (b) torsional modes [Eq. (50b)].

the decrease in the hydrodynamic function Γ_t for the higher order mode ($n=10$) is even weaker, with a reduction of only 7% in comparison to the fundamental torsional mode ($n=1$). Thus, variations in the effect of the fluid depend on the combined effects of the geometry and mode number of the cantilever. The relationships between the resonant frequencies in fluid and vacuum depend on the mode number n only through the normalized mode number κ, and Eqs. (10) and (13) become

$$\omega_{\text{fluid}}^{(n)} = \omega_{\text{vac}}^{(n)}\left[1 + \frac{\pi\rho b}{4\rho_c h}\Gamma_f(\kappa)\right]^{-1/2} \tag{49a}$$

for the flexural mode and

$$\omega_{\text{fluid}}^{(n)} = \omega_{\text{vac}}^{(n)}\left[1 + \frac{3\pi\rho b}{2\rho_c h}\Gamma_t(\kappa)\right]^{-1/2} \tag{49b}$$

for the torsional mode.

To facilitate computation for arbitrary κ, we now present approximate yet accurate formulas for the hydrodynamic functions that may be used in place of the exact analytical solutions, depending on the accuracy required. These are derived from the asymptotic results for small and large κ while minimizing the relative error for intermediate values of κ using a Padé approximant representation. The corresponding formulas for the flexural and torsional modes, respectively, are

$$\Gamma_f(\kappa) = \frac{1 + 0.742\,73\kappa + 0.148\,62\kappa^2}{1 + 0.742\,73\kappa + 0.350\,04\kappa^2 + 0.058\,364\kappa^3}, \tag{50a}$$

$$\Gamma_t(\kappa) = \frac{1}{16}\left(\frac{1 + 0.379\,22\kappa + 0.072\,912\kappa^2}{1 + 0.379\,22\kappa + 0.088\,056\kappa^2 + 0.010\,737\kappa^3}\right). \tag{50b}$$

The accuracies of these formulas are illustrated in Fig. 4,

from which we find that the maximum error in Eq. (50a) is 0.6% and the maximum error in Eq. (50b) is 0.3%. Both formulas also possess the correct and exact asymptotic behavior as $\kappa\to 0$ and $\kappa\to\infty$, and therefore can be used with confidence to accurately compute the hydrodynamic functions for all values of κ.

Finally, we comment briefly on the applicability of these results to microcantilevers, where the effects of viscosity can be important.[7] The critical parameter dictating the importance of viscosity is the Reynolds number

$$\text{Re} = \frac{\rho\omega X_0^2}{\eta}, \tag{51}$$

where ω is a characteristic radial frequency, ρ and η are the density and viscosity of the fluid, respectively, and X_0 is the dominant length scale of the flow around the cantilever. As discussed in Ref. 7, the effects of fluid viscosity are important provided $\text{Re}\lesssim O(1)$, which is typically the case for the fundamental mode of microcantilevers. However, as the mode number increases, so too does the resonant frequency and hence the Reynolds number Re. As such, an inviscid flow analysis is applicable to microcantilevers provided Re is large. This feature explains the discrepancies in the accuracy of the inviscid theory for lower order and higher order modes of microcantilevers, as measured experimentally in Ref. 16. In Ref. 16 it was suggested that these discrepancies are primarily dependent on the mode number. However, the above detailed derivation establishes that the theoretical formalism is valid regardless of mode number, provided the fluid can be considered to be inviscid. For the lower order modes examined in Ref. 16, the microcantilevers possess a Reynolds number of order unity indicating that viscous effects are important. Thus, the poor agreement found between inviscid theory and experiment for the lower order modes of microcantilevers is to be expected. However, for the higher order modes investigated in Ref. 16, the Reynolds number greatly exceeds unity and hence good agreement between inviscid theory and experiment would be expected, as was observed. This discussion therefore clarifies the role of mode number on the applicability of the inviscid formulation to microcantilevers.

IV. CONCLUSIONS

We have presented a detailed theoretical analysis of the resonant frequencies of rectangular cantilever beams immersed in fluid. The models presented are rigorously valid for arbitrary mode number and for cases where the fluid may be considered to be inviscid in nature. Consequently, the theory is directly applicable when the Reynolds number Re is large, as is usually the case for macroscale cantilevers. The present formulation extends the methodology of Elmer and Dreier[16] to the torsional modes, while yielding exact analytical solutions. Importantly, it was found that the resonant frequencies of the cantilever are unaffected by the fluid in the limit of infinite mode number, in contrast to low mode number cases. To facilitate computation, approximate yet simple and accurate analytical formulas were also presented, which are expected to be of value in practice. A summary of the key theoretical formulas is presented in Table I.
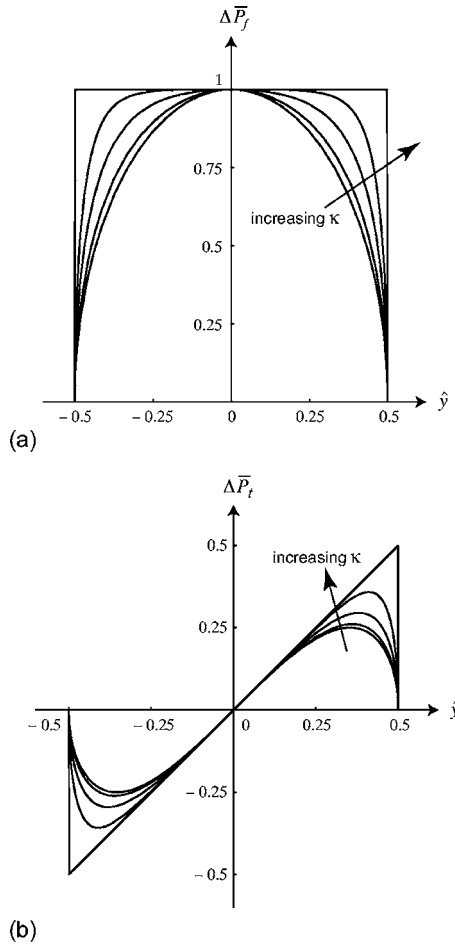
$$\Delta p(\hat{x}, \hat{y}|\omega) = \rho \omega^2 b Z_0 e^{i\kappa \hat{x}} \sum_{m=1}^{M} b_m \frac{2\hat{y}}{m} U_{2m-1}(\sqrt{1-4\hat{y}^2}),$$

$$(\text{A1b})$$

where the functions T and U are Chebyshev polynomials of the first and second kind,[20] respectively, and the scaled coordinates $\hat{x}$ and $\hat{y}$ are as defined in Sec. II. Note that unlike the total force acting on the beam, the pressure depends on all coefficients a_m and b_m, cf. Eqs. (A1), (31) and (42).

The pressure jump distributions for both the flexural and torsional modes are presented in Fig. 5 as a function of normalized mode number κ. Note that as κ increases, the pressure distributions in both cases become linear near the axis of the beam, i.e., $\hat{y}=0$. This is as expected, since the flow must become two dimensional with respect to the x and z directions in the limit as $\kappa \to \infty$. This contrasts to the limit as $\kappa \to 0$, where the flow is two dimensional with respect to the y and z directions. The corresponding asymptotic formulas in these limits are

$$\Delta p(\hat{x}, \hat{y}|\omega) = \rho \omega^2 Z_0 e^{i\kappa \hat{x}} \begin{cases} \sqrt{1-4\hat{y}^2} & : \kappa \to 0 \\ \dfrac{2}{\kappa} & : \kappa \to \infty \end{cases} \quad (\text{A2a})$$

for the flexural modes and

$$\Delta p(\hat{x}, \hat{y}|\omega) = \rho \omega^2 Z_0 e^{i\kappa \hat{x}} \begin{cases} \dfrac{1}{2}\hat{y}\sqrt{1-4\hat{y}^2} & : \kappa \to 0 \\ \dfrac{2\hat{y}}{\kappa} & : \kappa \to \infty \end{cases} \quad (\text{A2b})$$

for the torsional modes.

FIG. 5. Normalized pressure jump across beam as a function of normalized mode number $\kappa=0,3,7,15,\infty$. (a) Flexural modes $\Delta \bar{P}_f=\Delta p(\hat{x}, \hat{y}|\omega)/\Delta p(\hat{x}, 0|\omega)$ and (b) torsional modes $\Delta \bar{P}_t=\Delta p(\hat{x}, \hat{y}|\omega)/[\ \partial \Delta p(\hat{x}, \hat{y}|\omega)/\partial \hat{y}|_{\hat{y}=0}]$.

ACKNOWLEDGMENTS

APPENDIX

In this Appendix, we present explicit analytical formulas for the pressure jump across the surface of the cantilever beam, i.e., $\Delta p(x, y|\omega)=p(x, y, 0^-|\omega)-p(x, y, 0^+|\omega)$, where the pressure corresponds to its Fourier transformed quantity.

Using the ansatz described in Sec II, for the flexural modes we find

$$\Delta p(\hat{x}, \hat{y}|\omega) = \rho \omega^2 b Z_0 e^{i\kappa \hat{x}} \sum_{m=1}^{M} a_m \frac{2}{2m-1} T_{2m-1}(\sqrt{1-4\hat{y}^2}),$$

$$(\text{A1a})$$

whereas for the torsional modes

[1] R. Berger, Ch. Gerber, H. P. Land, and J. K. Gimzewski, Microelectron. Eng. **35**, 373 (1997).
[2] U. S. Lindholm, D. D. Kana, W.-H. Chu, and H. N. Abramson, J. Ship Res. **9**, 11 (1965).
[3] L. Landweber, J. Ship Res. **11**, 143 (1967).
[4] P. Kaleff, J. Ship Res. **27**, 103 (1983).
[5] G. Binnig, C. F. Quate, and Ch. Gerber, Phys. Rev. Lett. **56**, 930 (1986).
[6] C. H. Ho and Y. C. Tai, Annu. Rev. Fluid Mech. **30**, 579 (1998).
[7] J. E. Sader, J. Appl. Phys. **84**, 64 (1998).
[8] C. P. Green and J. E. Sader, J. Appl. Phys. **92**, 6262 (2002).
[9] M. R. Paul and M. C. Cross, Phys. Rev. Lett. **92**, 235501 (2004).
[10] C. P. Green and J. E. Sader, J. Appl. Phys. **98**, 114913 (2005).
[11] S. Basak, A. Raman, and S. V. Garimella, J. Appl. Phys. **99**, 114906 (2006).
[12] M. R. Paul, M. T. Clark, and M. C. Cross, Nanotechnology **17**, 4502 (2006).
[13] J. Dorignac, A. Kalinowski, S. Erramilli, and P. Mohanty, Phys. Rev. Lett. **96**, 186105 (2006).
[14] J. W. M. Chon, P. Mulvaney, and J. E. Sader, J. Appl. Phys. **87**, 3978 (2000).
[15] W.-H. Chu, Southwest Research Institute Technical Report No. 2, DTMB, Contract NObs–86396 (X), 1963 (unpublished).
[16] F.-J. Elmer and M. Dreier, J. Appl. Phys. **81**, 7709 (1997). For the flexural mode, the hydrodynamic function $\Gamma_f(\kappa)$, defined in Eq. (9) is related to Elmer's "master function" $f(\kappa)$, by $f(\kappa)=(\pi/16)\Gamma_f(\kappa)$,.
[17] G. K. Batchelor, *An Introduction to Fluid Dynamics* (Cambridge University Press, Cambridge, 1974).
[18] L. D. Landau and E. M. Lifshitz, *Theory of Elasticity* (Pergamon, Oxford, 1970).
[19] Y. L. Luke, *The Special Functions and Their Approximations* (Academic, New York, 1969).
[20] M. Abramowitz and I. A. Stegun, *Handbook of Mathematical Functions* (Dover, New York, 1972).